Journal of Power Sources 269 (2014) 396–402

Contents lists available at ScienceDirect

Journal of Power Sources

journal homepage: www.elsevier.com/locate/jpowsour

The influence of the carbonate species on $LiNi_{0.8}Co_{0.15}Al_{0.05}O_2$ surfaces for all-solid-state lithium ion battery performance

Heidy Visbal [a, 1], Satoshi Fujiki [a], Yuichi Aihara [a, *], Taku Watanabe [a], Youngsin Park [b], Seokgwang Doo [b]

[a] AR-3, Samsung R&D Institute Japan, Minoh Semba Center Bldg. 13F, Semba Nishi 2-1-11, Minoh, Osaka 562-0036, Japan
[b] Energy Lab, SAIT, Samsung Electronics Co., Ltd., 130, Samsung-ro, Yeongtong-gu, Suwon-si, Gyeonggi-do 443-803, Republic of Korea

HIGHLIGHTS

- Surface of NCA was analyzed by DRIFT and XPS to determine the adsorbed species.
- Carbonate unidentate was found to form on the NCA surface.
- The surface impurities significantly increased the charge transfer resistance.
- Importance of the surface treatment of NCA was demonstrated.

ARTICLE INFO

Article history:
Received 5 April 2014
Received in revised form
2 July 2014
Accepted 4 July 2014
Available online 11 July 2014

Keywords:
All solid-state lithium-ion batteries
Surface carbonate
Cathode material
Sulfide electrolyte
Surface resistance

ABSTRACT

The influence of selected carbonate species on $LiNi_{0.8}Co_{0.15}Al_{0.05}O_2$ (NCA) surface for all-solid-state lithium-ion battery (ASSB) with a sulfide based solid electrolyte was studied for its electrochemical properties, structural stabilities, and surface characteristics. The rated discharge performance improved with the reduction of the carbonate concentration on the NCA surface due to the decrease of the interface resistance. The species and coordination of the adsorbed carbonates on the NCA surface were analyzed by diffuse reflectance Fourier transformed infrared (DRIFT) spectroscopy. The coordination of the adsorbed carbonate anion was determined based on the degree of splitting of the ν_3(CO) stretching vibrations. It is found that the surface carbonate species exists in an unidentate coordination on the surface. They react with the sulfide electrolyte to form an irreversible passivation layer. This layer obstructs the charge transfer process at the cathode/electrolyte interface, and results in the rise of the interface resistance and drop of the rated discharge capability.

1. Introduction

Recently, *x*EVs, i.e., hybrid, plug-in hybrid and electric vehicles, have attracted considerable attention due to the marked increases in fuel costs and growing environmental concerns. For such applications, Lithium-ion batteries (LIBs) are considered to be the most promising device due to their large capacity, excellent rate capability, and low cost [1–3].

One of the major challenges for the LIBs is the mitigation of the safety concerns such as rapid temperature rises or even combustion of the batteries in these cars. All-solid-state lithium ion batteries (ASSBs) may provide a solution to the problem and extensive researches are being undertaken around the world [4,5]. A wide variety of solid state electrolytes have been studied so far to improve their lithium-ion conductivity [6–12]. Sulfide-based solid electrolytes such as thio-LiSICON $Li_{3.25}Ge_{0.25}P_{0.75}S_4$, xLi_2S–$(1-x)P_2S_5$, and $Li_{10}GeP_2S_{12}$ exhibit high lithium ion conductivities of the order of 10^{-3} to 10^{-2} S cm^{-1} at room temperature [4,13,14], approaching to the ionic conductivity of organic electrolytes.

However, there are some critical issues to overcome before realizing practical ASSBs using with sulfide solid electrolyte. The first issue is to make good physical contacts between the active material and solid electrolyte. Most of the ASSBs require an external pressure during charge–discharge process to maintain the interface contacts, because the expansion and contraction of the active materials sometimes result in poor contact of the materials and

* Corresponding author.
E-mail addresses: yuichi.aihara@samsung.com, yuichi.aihara@nifty.com (Y. Aihara).
[1] Present address: Faculty of Engineering, Kyoto University, Kyoto daigaku-katsura, Nishikyo-ku, Kyoto 615-8530, Japan.

http://dx.doi.org/10.1016/j.jpowsour.2014.07.021
0378-7753/

increase the resistance. Recently, some progress has been made in this direction, and a large size ASSBs using $80Li_2S–20P_2S_5$ electrolytes were developed using a polymer binder [15]. It showed stable charge–discharge cycle without an application of external pressure [15].

The second issue is to maintain the interface chemical stability between the active material and sulfide solid electrolyte. It has been reported that the mutual diffusion of atoms occurs between the oxygen of the active material and the sulfur of the electrolyte, making high resistance interface layer [16] or highly resistive layer originated in a Schottky barrier at the interface [17–19]. Some studies have been conducted to modify the interface in order to mitigate this issue. A thin buffer layer of $LiNbO_3$ [19], SiO_2 [20] or $Li_4Ti_5O_{12}$ [21] was placed between the $LiCoO_2$ cathode material and the sulfide solid electrolyte in order to reduce the interfacial resistance [15–21]. However, there are only a few reports on coating effects on Ni-based cathode active materials. Machida et al., has reported that ZrO_2 coating on the $LiNi_{1/3}Mn_{1/3}Co_{1/3}O_2$ cathode materials works as a buffer layer to suppress the formation of high-resistance layers [16].

Ni based cathode materials are known to have several serious problems when they are used in conventional liquid LIBs. These materials absorb moisture and Li_2CO_3/LiOH impurities on the surface when they are exposed to the air [22–27]. Some studies have shown the correlations between electrochemical properties of a LIB and Li_2CO_3 contamination in liquid electrolytes [24,28,29]. Recent results suggest that Li_2CO_3 causes the performance loss of Ni-based cathode materials in LIBs [25,26,30]. The formation of Li_2CO_3 during storage is often attributed to the presence of H_2O and CO_2 in air. Trace amounts of H_2O and CO_2 in air can be adsorbed on the surface of the active material and react with lithium ions to form a layer of lithium carbonate [30]. However, as Liu et al. reported, Li_2CO_3 is not the only surface species causing performance loss of the batteries. In fact, hydroxyls, bicarbonates, carbonates, crystalline Li_2CO_3, and Ni–O like species were identified to be the major species formed on the stored Ni-based materials based on TG measurements [30]. They also reported that below 500 °C the weight loss was due to desorption of those species beside Li_2CO_3 as it decomposes around 700 °C. However, to the best of our knowledge, there has been no report on the correlation of the effect of the surface impurities including adsorbed carbonates and the electrochemical performance of an ASSB with sulfide solid electrolyte. Therefore, there is an urgent need for deeper understanding of the surface condition of Ni-based cathode materials and its reactions with the sulfide solid electrolyte.

A well-known technique for obtaining the surface localized infrared spectra of powdered samples is diffuse reflectance infrared Fourier transform (DRIFT) spectrometry. This technique allows one to obtain IR spectra of chemical species at the surface of the samples as it focuses on the shallow region of the sample unlike a transmission IR. Thus, it can provide chemical and structural information for all types of solid surfaces.

For this purpose, we investigated the impact of the surface absorbed carbonates and impurities on the oxide cathode material $LiNi_{0.8}Co_{0.15}Al_{0.05}O_2$ (NCA) using the DRIFT. The effect of eliminating the carbonate species and contaminations on the NCA surface was examined through the electrochemical properties of the sulfide based ASSB.

2. Experimental

2.1. Surface characterization

The surface of NCA powder was characterized by DRIFT and X-ray photoelectron spectroscopy (XPS). The DRIFT spectra were obtained by using an FTIR spectrometer (FT/IR-6200, JASCO) equipped with a triglycine sulfate (TGS) detector, DRIFT accessory (JASCO, Model no. DR-600A). Each spectrum was composed of 128 scans at 4 cm^{-1} resolution. The sample and background spectra were collected in a power mode and stored as single beam spectra for further processing. To increase the signal-to-noise ratio of the spectrum from the NCA powder and to avoid influences of water absorbed on KBr, the sample was placed in a micro sample holder without diluting in KBr. The DRIFT spectra of all powders were recorded under atmosphere and $4.0–5.0 \times 10^{-2}$ Pa of vacuum in a vacuum chamber (JASCO, Model no. DR-600A) equipped with a turbo molecular pump and sorption pump. The samples were also heated in-situ in a dome with BaF windows under vacuum at 10 K min^{-1} up to 300 °C. Three samples were prepared for each condition. DRIFT spectra of three different portions of the samples in the range of 4000–400 cm^{-1} were obtained in dry air atmosphere with no dilution. For each spectrum, 256 scans were accumulated at a resolution of 4 cm^{-1}. Spectral processing such as baseline adjustment and smoothing were performed using an OMNIC software package. The second derivative spectra derived from the absorbance spectra were deconvoluted and the peaks quantified using a Jandel peak separation and analysis software PeakFit™ 4.0 (AISN Software Inc., USA) in log (1/R) units. Peak fitting was carried out until squared correlation coefficients with r^2 greater than 0.999 and best F standard values were obtained.

XPS measurements were performed on a PHI 5000 VersaProbe (ULVAC-PHI) with monochromatic Al Kα (1.4866 keV). A sealed vessel was used to transfer the sample from the glove box to the analyzer chamber in order to avoid air exposure. The powder samples were tightly pressed onto an indium foil instead of carbon tape to avoid the influence on the carbon peak.

To verify the crystallinity and impurities of the samples, the powder X-ray diffraction (XRD) pattern was obtained using an Empyrean XRD system (CuKα, 45 kV, 40 mA, PANalytical, Almelo). An Ar-gas-filled sample holder was used during the measurement.

2.2. Electrochemical evaluation

To examine the effect of surface carbonates and/or impurities on the electrochemical performance of sulfide based ASSB, two samples were prepared as follows:

2.2.1. Low clean level (LCL)

NCA (D_{50} = ca. 5 μm) powder was heated at 80 °C under a rotary pump vacuum for 24 h. After the drying, the sample holder was opened in a dry room at a dew point of approximately −50 °C. Then the powder was transferred to an argon globe box for cell preparation.

2.2.2. High clean level (HCL)

In order to remove surface impurities, NCA (D_{50} = ca. 5 μm) powder was heated in a glass sealed tube at 250 °C in vacuum for 1 h and was transferred to the argon glove box without any contact with the air.

The amorphous $Li_2S–P_2S_5$ (80:20 mol%) electrolyte was prepared by high energy ball milling in accordance to the previous paper [15,31]. To prepare the cell, 100 mg of the electrolyte $Li_2S–P_2S_5$ (80:20 mol%) was first placed into a Teflon® die of 13 mm in diameter to make an electrolyte layer. It was hand-pressed to shape the material into a pellet. Then, the cathode composites were prepared by mixing the cathode active materials with vapor grown carbon fiber (VCF, fiber diameter = ca. 200–500 nm, length = ca. 5–10 μm) and the electrolyte $Li_2S–P_2S_5$ (80:20 mol%) at the ratio of 60 : 5 : 35 in weight, respectively. 15 mg of the above cathode composite powder was uniformly spread onto the electrolyte

pellet, and a stainless-steel (SUS316) cylinder as the current collector was stacked on the cathode. The anode composite was prepared by mixing synthetic graphite (spherical shape, D_{50} = ca. 15 μm) with VCF, and Li_2S–P_2S_5 (80:20 mol%) in a weight ratio of 60:5:35. Then, the cell was then turned upside-down, and 15 mg of the anode composite was similarly placed on the other side of the electrolyte layer. After the anode current collector (SUS316 cylinder) was put onto the anode composite, all the cell components were compressed using a hydraulic press at 4 tons. Then, the cell components with insulator Teflon® housing and the current collectors were finally mounted on a vessel which is separated by an O-ring, and was closed by a torque control wrench at 3 Nm^{-1} for keeping the cell displacement. All the steps were carried out in an Ar filled glove box. Further details of the cell fabrication are given in another paper [15,31].

Electrochemical properties of the NCA based cathode were investigated by galvanostatic charge–discharge tests and electrochemical impedance spectroscopy (EIS). The charge and discharge tests were performed at 25 °C using a multi-channel potentiogalvanostat (PS-08, Tohogiken). The initial charge–discharge cycle was performed at 0.05C in constant current (CC) mode. The charge and discharge cutoff potentials were 4.0 and 2.8 V, respectively. A frequency response analyzer, Solartron 1260 equipped with an electrochemical interface, Solartron 1287 (Solartron Analytical, Hampshire), was used for the EIS measurement. The EIS was performed after initial charge (SOC = 100). The impedance spectra were obtained by applying AC perturbation signal of 10 mV to the cell open circuit potential within a frequency range between 10^6 and 10^{-1} Hz. For checking the rated discharge performance of the cells, the cells were discharged at various C-rates, after the cells were charged to 4.0 V by 0.5C (CC) combined with a constant voltage (CV) until the current was sufficiently decayed to 0.01C or the CV time reached to 15 h.

3. Results and discussion

3.1. Characterization results

The crystal structures of the LCL and HCL NCA powder samples were evaluated using the XRD. The collected XRD patters are shown in Fig. 1. Both samples are single phase and isostructural with $LiNiO_2$ with $R\bar{3}m$ space group [27,28]. There is no obvious difference between the both powder spectra. This result indicates that heating the sample at 250 °C in vacuum for 1 h does not alter the crystal structure and lattice constants of the NCA.

Fig. 2 is the conventional scale DRIFT spectra of the NCA powder in vacuum at different temperatures in the region of 2000 to 1000 cm^{-1}. Two main peaks were found in the region between 1600 and 1400 cm^{-1} from the sample below 150 °C. These band intensities decreased with the increase of the temperature and were no longer visible above 250 °C. These peaks are assigned to an ionic carbonate structure. The carbonate anion, CO_3^{2-}, gives rise to two bands: a strong asymmetrical stretching band, ν_{as} (COO^-) and a symmetric band ν_s (COO^-) around 1650–1450 cm^{-1} [32–39] for several metal oxide complex.

Binding mode of the surface carbonate species can be classified in 4 categories; free carbonate ion, unidentate carbonate, bidentate carbonate, and organic carbonates. A resume of the bands for each category of the carbonates can be found in the literature [37,38]. Identification of the chemisorbed carbonate is conventionally done on the basis of the splitting of ν_3 ($\Delta\nu_3$) of the asymmetric CO stretching. The use of $\Delta\nu_3$ for distinguishing between the monodentate and bidentate carboxylate coordinations in metal complexes was first proposed by Nakamoto et al. [33,34]. Bidentate carbonate complexes generally exhibit the Δ-values {ν_{as}(COO–)–ν_s(COO–)} greater than ionic complexes in the range of Δ~200–300 cm^{-1}. For unidentate carbonate complexes, the same quantity is much less (Δ~30–80 cm^{-1}) than those of the ionic complexes. This reflects the fact that the effect of coordination is stronger in the bidentate than in the unidentate, therefore a lager CO splitting is observed.

As shown in Fig. 2, our NCA samples presents two CO bands located at 1493 cm^{-1} and 1430 cm^{-1} corresponding to ν_{as}(COO–) and ν_s(COO–) respectively. The CO splitting gives a small value of $\Delta\nu_3 = 63$. Therefore, we assume that the binding of the CO_3^{2-} ion to the NCA surface has the unidentate coordination. Considering the surface of NCA, carbon dioxide can be adsorbed only to lithium, nickel or unsaturated surface oxygen. Since this adsorbed carbonate species can be eliminated around 250 °C, we assume that the surface carbonate species is simply adsorbed on the surface atoms, rather than forming another compound like Li_2CO_3. Li_2CO_3 is a stable compound and possible to form in the presence of Li and CO_2. However, it decomposes around 700 °C, much higher than the observed carbonate desorption temperature of 250 °C in our sample. Therefore, we can safely assume that Li_2CO_3 would not play any important role in this sample and carbonate species exist on the surface of NCA as adsorbed species. Therefore, the surface carbonate species are expected to form by the coordination of the CO_2 carbon to coordinately unsaturated surface oxygen or one of the molecular oxygen atoms to a coordinately unsaturated surface nickel cation. CO_2 is an amphoteric compound able to behave either as an acid molecule when the carbon atom binds to surface oxygen

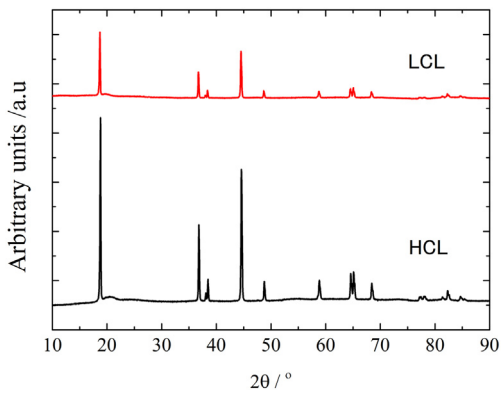

Fig. 1. XRD patterns of the NCA powders at different drying conditions.

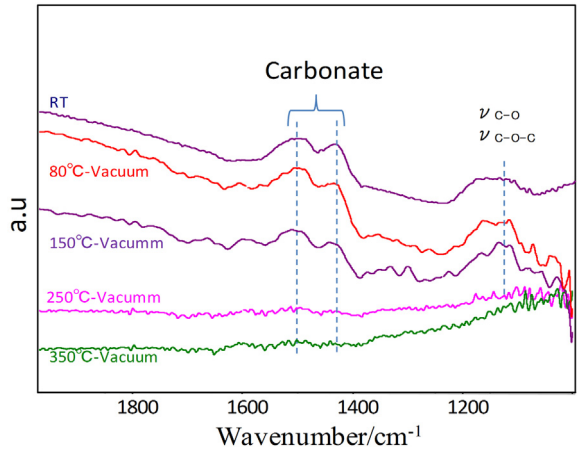

Fig. 2. DRIFT spectra for NCA powder at different heating temperatures in vacuum.

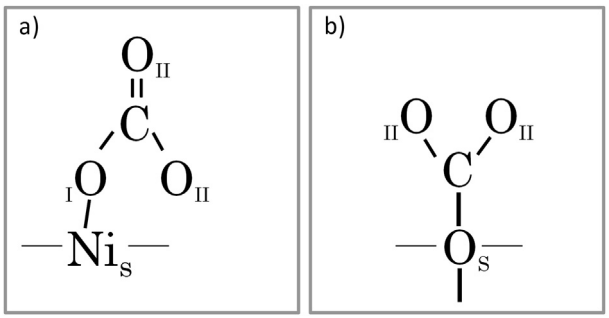

Fig. 3. Schematic representations of the unidentate adsorbed carbonate species on the NCA surface. S (subscript), O_I and O_{II} refer to surface atoms, a molecular oxygen atoms coordinated unsaturated surface nickel cation and a molecular oxygen of CO_2 molecule, respectively.

atom or as a weak base when it binds to the surface cations through the electron pairs of the oxygen atoms [40]. It is reasonable to expect that terminal surface oxygen to interact with the electropositive carbon atom in CO_2 rather than the oxygen atoms of a CO_2 molecule [39]. Also, the interaction between two closed-shell oxygen atoms (terminal oxygen on the surface and molecular oxygen on the CO_2 molecule) will be expected to give rise to any significant attractive interaction, and would more likely give a short-range interaction that is repulsive in nature [39].

Schematic representations of the possible unidentate carbonate coordinations at the NCA surface are shown in Fig. 3. Fig. 3a) is a model representing CO_2 adsorbed to molecular oxygen atoms to a coordinately unsaturated surface nickel cation, and Fig. 3b) represents a CO_2 adsorbed to coordinately unsaturated surface oxygen. Since the surface oxygen is directly bound to a Ni atom, both types of coordinations belong to the nickel carbonates and the difference would not appear in our DRIFT spectra.

Fig. 4 shows the C1s and O1s photoelectrons XPS spectra of the LCL and HCL samples. For the C1s photoelectron peak, the main peak for the LCL sample was at 289.5 eV corresponding to a carboxylic structure [40]. Additionally, a carbonate (CO_3^{2-}) peak was observed around 292.0 eV. On the contrary, the HCL sample showed no such peak around the same energy range, and it indicates that much less quantity of the carboxylic component exist on the surface. The XPS spectra were fitted by multiple Gaussian profiles and the areas under the peaks are summarized in Table 1. It is clear that the HCL sample have smaller amount of carbonate (CO_3^{2-}) and carboxyl (COO^-) groups at the surface of NCA than the LCL sample.

Table 1
Summary of the C1s photoelectron peak fitting. The energies indicate the binding energies of the corresponding peaks. The values of the table for C–H, COO^-, CO_3^{2-} represent the area under the fitted curves. The right two columns are the ratio of the areas under the curves.

	C–H peak	COO^- peak	CO_3^{2-} peak	CO_3^{2-}/C–H	COO^-/C–H
	284.7 eV	289.5 eV	291.5 eV	291.5 eV peak/ 284.7 eV peak	289.5 eV peak/ 284.7 eV peak
HCL	33.4	52.5	14.1	0.4	0.3
LCL	19.7	53.4	27.0	1.4	0.5

For the O 1s photoelectron peak, the main peaks for both samples are found at 531.5 eV corresponding to adsorbed hydroxyl and carbonate species [41]. Another peak around 528.0 eV is observed in both samples, corresponding to lattice oxygen. It is clear that the HCL sample shows a larger amount of the peak corresponding to metal-oxygen at 528.2 eV in comparison with the LCL sample. Thus the HCL NCA surface is clean and most of the terminal oxygen ions are bonded to Ni cations at the surface. The LCL sample shows the dominating peak at 531.5 eV, and the peak at low binding energy (528.2 eV) corresponding to lattice oxygen is very small compared to the HCL sample. It means that the lattice oxygen of this sample surface is mostly covered by some adsorbed species. This result suggests that drying at 80 °C for 24 h and open in dry room is not enough to reduce the surface impurities for this material. As supported by the DRIFT spectra, heating above 250 °C in vacuum is necessary to remove the surface impurities on the NCA powder surface.

3.2. Electrochemical evaluation

After the sample characterization was completed, we evaluated the electrochemical performances of the LCL and HCL NCA samples.

Fig. 5 shows the initial charge–discharge curves of the LCL and HCL samples. The charge/discharge capacity values and the initial Coulombic efficiency (ICE) for both samples are given in Table 2. The discharge capacities of the LCL and HCL samples were 104 and 119 mAh g^{-1}, respectively. This marked increase in the capacity is ascribed to the cleaner surface condition of the HCL sample. Generally speaking, poor initial Coulombic efficiency is often observed on sulfide based ASSBs due to its side reaction at the cathode material. This is closely related to the difference of the NCA/sulfide electrolyte interface between the two samples. Since the ICE increased from 58.4% to 63.6% by changing the drying

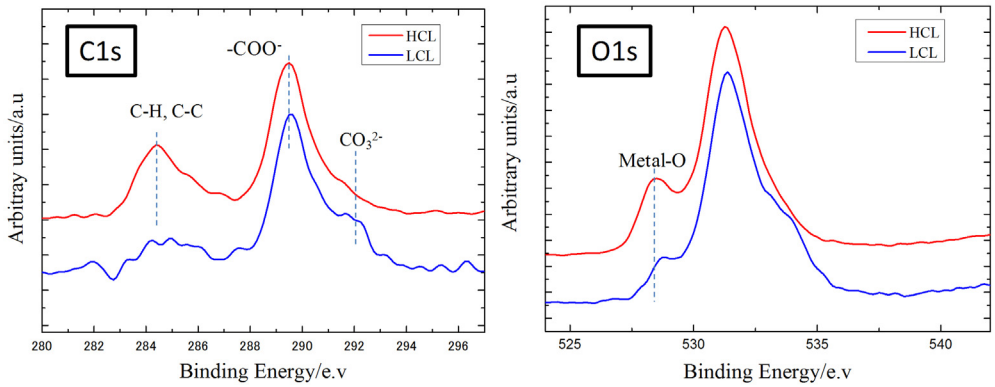

Fig. 4. C1s and O1s photoelectron peak under different dry conditions.

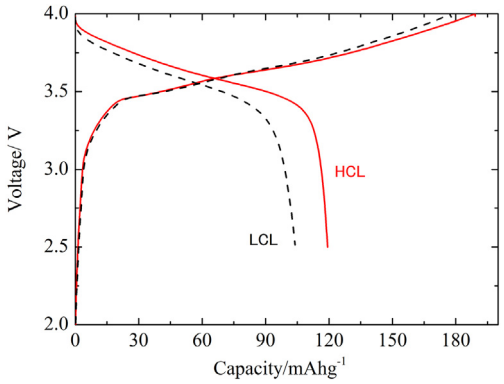

Fig. 5. 1st cycle charge–discharge curve for the NCA powder dried at different conditions.

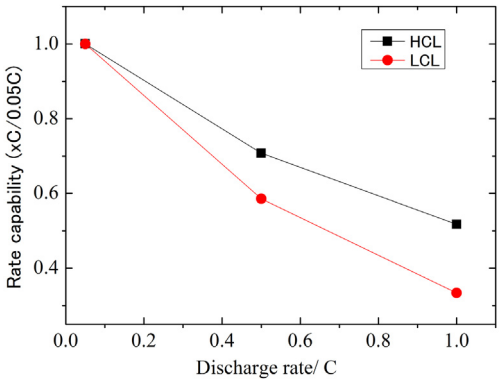

Fig. 7. Rate performance of the cell using the NCA powder dried at different conditions. The values were normalized by each discharge capacity at 0.05C.

Table 2
Initial charge discharge capacities given in two different drying conditions.

	Charge/mAh g^{-1}	Discharge/mAh g^{-1}	ICE/%
NCA – LCL	178	104	58.4
NCA – HCL	187	119	63.6

condition, presumably, the existence of the carbonate species affected the process of the side reaction. From these results we can deduce that the carbonate compounds at the surface significantly affects the electrochemical properties at the charge–discharge process. To improve the ICE, both elimination of the carbonates from the NCA surface and formation of the protection layer may be required.

Next, the effect of the charge–discharge rate was studied and the results are shown in Fig. 6. The C-rate was set to 0.05C, 0.5C, and 1C for the discharging cycle. The charging was done at 0.5C at constant voltage until the cutoff current of 0.01C was reached. The rated capacity was clearly improved especially at the higher discharge rate. This is summarized in Fig. 7. At 1.0C, the improvement of the capacity was increased by approximately 20% of the maximum capacity at 0.05C.

Finally, the analysis of the cell resistance was performed by the AC impedance measurement. Comparison of the Nyquist plot of the HCL and LCL samples is shown in Fig. 8. Each spectrum consisted of a solution resistance above 173 kHz, a semi-circle in the high-frequency region (c.a. >2.6 Hz) and a straight line in the lower-frequency region below 2.6 Hz. The semi-circle and the straight line correspond to the cell kinetics including both cathode and anode charge transfer resistances and diffusive component, so-called Warburg impedance, respectively. According to our previous work [19], the cell impedance is mainly attributed to the cathode impedance, especially due to the charge-transfer. The measured impedance indicated that the resistances obtained from the semi-circles for the LCL and HCL samples were 416 Ω and 222 Ω, respectively. The plot consists of anode and cathode charge transfer resistances, and the difference is mostly originated from the cathode charge transfer process since the same anode is adopted in each cell. It is well known that a buffer layer is required to maintain the cathode/sulfide electrolyte interface in a solid state battery [15–21]. The resistance is nearly halved by the cleaner interface produced by the high temperature and vacuum; therefore, this result indicated that the nature of the high impedance is not only originated in the side reaction between cathode material and sulfide electrolyte, but also the impurities mainly based on the adsorbed species on the cathode surface. At de-lithiated stated, it shows a reduction of the interfacial resistance corresponding to the cathode charge-transfer mechanism when the NCA powder is free of carbonate and impurities at the surface as shown by DRIFT and XPS results. These results show that the presence of the carbonates and impurities on the NCA surface causes the increase of the interface resistance between cathode and sulfide solid electrolyte. The adsorbed carbonate compounds at the surface significantly affect the interface resistance, probably because the carbonates or impurities surface groups could form an impediment against lithium ion diffusion at the charge–discharge process.

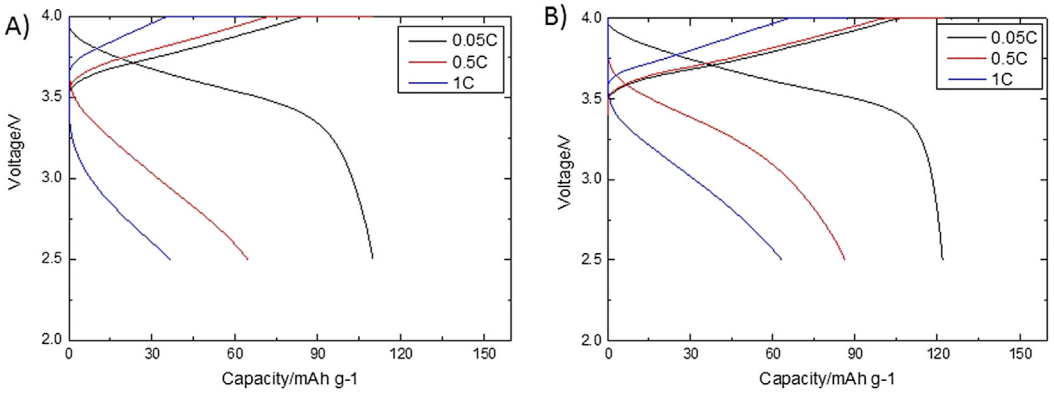

Fig. 6. Charge/discharge curves of A) LCL and B) HCL for different discharge rates at 25 °C. The constant current combined with the constant voltage (4.0 V) mode was adopted for the charge process.

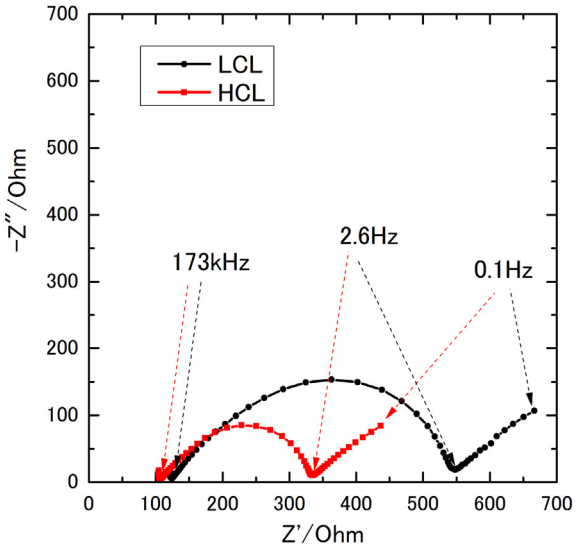

Fig. 8. Nyquist plot for the cells using the NCA powder dried at different conditions.

Above results suggests that the improvement of the electrochemical properties (rate capability, impedance and discharge capacity) is most likely due to the elimination of surface carbonate impurities at high temperature in vacuum. Reactions between NCA and the atmosphere include various physical and chemical adsorption and possible direct redox reactions between the bulk material and atmosphere. The carbonate and other surface impurity layers are electrochemically inactive to lithium intercalation/deintercalation, therefore at high rate the effect is more pronounced at the cathode surface.

Based on the experimental data obtained, we propose two possibilities for the mechanism of how the adsorbed carbonate and impurity could affect the electrochemical properties at the sulfide electrolyte in an all solid state battery. The first possibility is based on the assumption that the impurity layer of the carbonate on the NCA surface simply obstructs the Li-ion transport at the interface. This increases the interfacial resistance and decrease the rate capability. In this case, no significant reactions between the surface impurities and solid electrolyte are assumed. A schematic representation is in Fig. 9a)). The second possibility is that the carbonate group on the NCA surface reacts with the sulfide electrolyte to form an irreversible passivation byproduct. A representation of this possibility is represented in Fig. 9b)). In this case, the byproduct layer can cause a hindrance to the Li-ion transport at the interface. Both possibilities could occur simultaneously and affect the electrochemical properties in the sulfide based solid batteries.

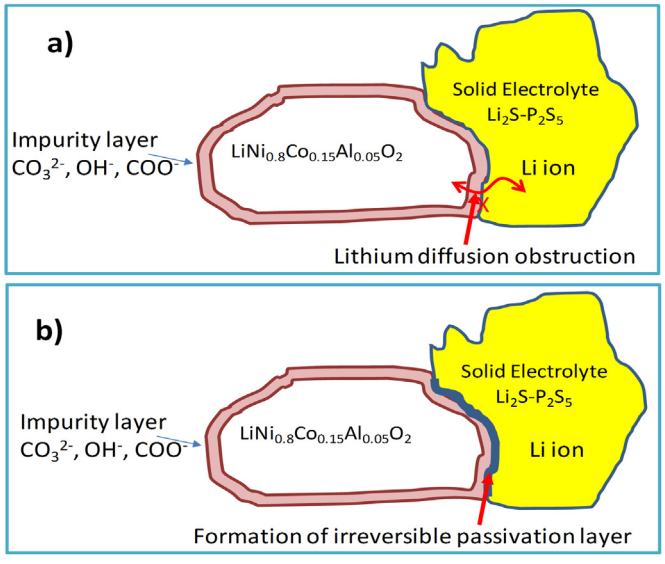

Fig. 9. Schematic representation of the NCA/solid electrolyte interface when the NCA surface is cover by CO_3^{2-} and or impurities.

We showed for first time that the surface impurities at the surface of cathode active particle affects profoundly the electrochemical properties in the sulfide based solid electrolyte batteries. The suppression of this surface impurities layer by the heat treatment under vacuum and/or a surface coating can help improve the electrochemical performance of the all-solid-state battery.

4. Conclusions

In this work, we found that the presence of the carbonates and other carbon originated impurities on the NCA surface affects the electrochemical charge transfer process on sulfide in all solid state batteries. It was verified that the carbonate layer formed on the NCA surface under the LCL condition, and it could be removed by shifting to the HCL condition. The change on the surface condition was analyzed by DRIFT and XPS.

The surface impurity layer of the carbonates was found to obstruct the charge transfer process at the cathode/solid electrolyte interface, and therefore the interface resistance increased and the rate capability decreased. The carbonate group on the NCA surface could also impede the lithium diffusion at the interface or react with the sulfide electrolyte and form irreversible passivation byproduct. Although further studies are needed to determine the exact mechanism and nature of the cathode-electrolyte interface, we clarified the impact of the surface treatment and surface carbonate species.

References

[1] J. Shim, R. Kostecki, T. Richardson, X. Song, K.A. Striebel, J. Power Sources 112 (2002) 222–230.
[2] R. Kostecki, F. McLarnon, Electrochem. Solid-State Lett. 7 (2004) A380–A383.
[3] M.-H. Kim, H.-S. Shin, D. Shin, Y.-K. Sun, J. Power Sources 159 (2006) 1328–1333.
[4] R. Kanno, M. Murayama, J. Electrochem. Soc. 14 (2001) A742–A746.
[5] K. Takada, N. Ohta, L. Zhang, K. Fukuda, I. Sakaguchi, R. Ma, M. Osada, T. Sasaki, Solid State Ionics 179 (2008) 1333–1337.
[6] S. Stramare, V. Thangadurai, W. Weppner, Chem. Mater. 15 (2003) 3974–3990.
[7] J.S. Thokchom, N. Gupta, B. Kumar, J. Electrochem. Soc. 155 (2008) A915–A920.
[8] J.B. Goodenough, H.Y.-P. Hong, J.A. Kafalas, Mater. Res. Bull. 11 (1976) 203–220.
[9] H.Y.-P. Hong, Mater. Res. Bull. 13 (1978) 117–124.
[10] M.A. Subramanian, R. Subramanian, A. Clearfield, Solid State Ionics 18&19 (1986) 562–569.
[11] H. Aono, E. Sugimoto, Y. Sadaoka, N. Imanaka, G. Adachi, J. Electrochem. Soc. 136 (1989) 590–591.
[12] R. Murugan, V. Thangadurai, W. Weppner, Angew. Chem. Int. Ed. 46 (2007) 7778–7781.
[13] F. Mizuno, A. Hayashi, K. Tadanaga, M. Tatsumisago, Adv. Mater. 17 (2005) 918–921.
[14] N. Kamaya, K. Homma, Y. Yamakawa, M. Hirayama, R. Kanno, M. Yonemura, T. Kamiyama, Y. Kato, S. Hama, K. Kawamoto, Nat. Mater. 10 (2011) 682–686.
[15] S. Ito, S. Fujiki, T. Yamada, Y. Aihara, Y. Park, T.Y. Kim, S.-W. Baek, J.-M. Lee, S. Doo, N. Machida, J. Power Sources 248 (2014) 943–950.
[16] N. Machida, J. Kashiwagi, M. Naito, T. Shigematsu, Solid State Ionics 225 (2012) 354–358.
[17] K. Takada, Acta Mater. 61 (2013) 759–770.
[18] Y. Seino, T. Ohta, K. Takada, J. Power Sources 196 (2011) 6488–6492.
[19] N. Ohta, K. Takada, I. Sakaguchi, L. Zhang, R. Ma, K. Fukuda, M. Okada, T. Sasaki, Electrochem. Commun. 9 (2007) 1486–1490.
[20] A. Sakuda, H. Kitaura, A. Hayashi, K. Tadanaga, M. Tatsumisago, Electrochem. Solid-State Lett. 11 (2008) A1–A3.

[21] N. Ohta, K. Takada, L. Zhang, R. Ma, M. Osada, T. Sasaki, Adv. Mater. 18 (2006) 2226–2229.
[22] K. Matsumoto, R. Kuzuo, K. Takeya, A. Yamanaka, J. Power Sources 81/82 (1999) 558–561.
[23] R. Moshtev, P. Zlatilova, S. vasilev, I. Bakalova, A. Kozawa, J. Power Sources 81/82 (1999) 434–441.
[24] A.M. Andersson, D.P. Abraham, R. Haasch, S. Maclaren, J. Liu, K. Amine, J. Electrochem. Soc. 149 (2002) A1358–A1369.
[25] G.V. Zhuang, G. Chen, J. Shim, X. Song, P.N. Ross, T.J. Richardson, J. Power Sources 134 (2004) 293–297.
[26] J. Kim, Y. Hong, K.S. Ryu, M.G. Kim, J. Cho, Electrochem. Solid-State Lett. 9 (2006) A19–A23.
[27] H.S. Liu, J. Li, Z.R. Zhang, Z.L. Gong, Y. Yang, Electrochem. Solid-State Lett. 7 (2004) A190–A193.
[28] J. Eom, M.G. Kim, J. Cho, J. Electrochem. Soc. 155 (2008) A239–A245.
[29] Y. Kim, J. Cho, J. Electrochem. Soc. 154 (2008) A495–A499.
[30] H. Liu, Y. Yang, J. Zhang, J. Power Sources 162 (2006) 644–650.
[31] M. Agostini, Y. Aihara, T. Yamada, B. Scrosatti, J. Hassoun, Solid State Ionics 244 (2013) 48–51.
[32] R.M. Silverstein, F.X. Webster, Spectrometric Identification of Organic Compounds, John Wiley Sons, Inc., New York, 1996, pp. 136–140. Silverstein R.M. and Webster F.X., "Spectrometric Identification of Organic Compounds", John Wiley and Sons, Inc., (1996) 136-140 Silverstein R.M. and Webster F.X., Spectrometric Identification of Organic Compounds, John Wiley and Sons, Inc., (1996) 136–140.
[33] K. Nakamoto, Infrared and Raman Spectra of Inorganic and Coordination Compounds, Wiley, New York, 1997, pp. 252–254.
[34] J. Fujita, A.E. Martell, K. Nakamoto, J. Chem. Phys. 36 (1962) 339–345.
[35] B.M. Gatehouse, S.E. Livingstone, R.S. Nyholm, J. Chem. Soc. (1958) 3137–3142.
[36] J.A. Goldsmith, S.D. Ross, Spectrochim. Acta 24A (1968) 993–998.
[37] H. Wijnja, C.P. Schulthess, Spectrochim. Acta A 55 (1999) 861–872.
[38] G. Busca, V. Lorenzelli, Mater. Chem. 7 (1982) 89–126.
[39] M. Abee, S.C. York, D.F. Cox, J. Phys. Chem. B 105 (2001) 7755–7761.
[40] R. Hammami, A. Dhouib, S. Fernandez, C. Minot, Catal. Today 139 (2008) 227–233.
[41] C.D. Wagner, W.M. Riggs, L.E. Davis, J.F. Moulder, G.E. Mullenberg, Handbook of X-ray Photoelectron Spectroscopy, 1979. Minessota.